Supporting Information

Understanding Fluoroethylene Carbonate and Vinylene Carbonate Based Electrolytes for Si Anodes in Lithium Ion Batteries with NMR Spectroscopy

Yanting Jin,[†] Nis-Julian H. Kneusels,[†] Lauren E. Marbella,[†] Elizabeth Castillo-Martínez,[†] Pieter C. M. M. Magusin,[†] Robert S. Weatherup,[†] Erlendur Jónsson,[†‡] Tao Liu,[†] Subhradip Paul,[§] and Clare P. Grey*[,†]

[†]Department of Chemistry, University of Cambridge, Lensfield Road, Cambridge CB2 1EW, United Kingdom

‡Department of Physics, Chalmers University of Technology, Gothenburg, 41296, Sweden

[§]DNP MAS NMR Facility, Sir Peter Mansfield Magnetic Resonance Centre, University of Nottingham, Nottingham NG7 2RD, United Kingdom

Table of Contents

S1: Experimental details

Materials

Battery grade LP30 electrolyte, FEC and VC were obtained from Sigma-Aldrich. The $LiPF_6$ salt was obtained from Aldrich. DNP solvent TCE (Sigma Aldrich) was dried over molecular sieves to remove water. TEKPol radical were kindly provided by the DNP facility in Nottingham. NMR experiments were used to estimate water content using small quantities 30 μl of NMR-grade ^{2}H-DMSO and 0.7 ml of FEC, VC or LP30. Although the ^{2}H-DMSO contains trace amounts (15 – 35 ppm) of water complicating the analysis, the natural abundance enriched electrolytes all contained < 120 ppm H_2O.

Electrochemical Impedance Spectroscopy (EIS)

The cells were rested in open circuit voltage for 15 h to reach equilibrium before EIS data was collected. All EIS measurements were made using a Biologic VMP3 electrochemical station at room temperature (18 ± 3 °C) using an excitation signal of 10.0 mV amplitude and a frequency range from 1 MHz to 0.1 Hz.

XPS

XPS spectra were acquired using the scanning photoemission microscopy (SPEM) instrument at the Escamicroscopy beamline of the Elettra synchrotron facility (Trieste, Italy). Measurements were performed using a 1075 eV X-ray beam that is defocussed to give a ~80 μm diameter spot size. Photoelectrons were collected with a SPECS-PHOIBOS 100 hemispherical electron energy analyzer with an in-house customized multichannel plate detector. The binding energy (BE) scale was calibrated on the hydrocarbon C 1s peak at 284.5 eV. All spectra were collected with 30 scans. Samples were transferred using sealed polyethylene glove bags to avoid air exposure.

FTIR

Dried silicon nanowire (SiNWs) electrodes were characterized using a FTIR spectrometer (Agilent, Cary 630) inside an argon-filled glovebox, in attenuated total reflection (ATR) mode on a diamond crystal. Each FTIR spectrum was acquired with a resolution of 4 cm^{-1} with 32 scans with the range from 600 to 4000 cm^{-1}.

Solution NMR experimental details

The glass fibre separator (containing ~ 0.1 ml electrolyte) was extracted from cycled coin cell, then soaked in ~0.6 ml deuterated ACN solvent for 5-10 min to extract the cycled electrolyte. The solution was later transferred into an air-tight J-Y NMR tube for solution NMR measurement. Sample preparation was carried out in glovebox.

1D $^{13}C\{^1H\}$ NMR spectra were recorded using either the standard 30° observe pulse, using 'waltz16' pulse-gated decoupling or with the udeft[1] sequence on a 500 MHz Bruker Avance III HD, with a DCH (carbon observe) cryoprobe. In cases where ^{1}H decoupling artifacts were too intrusive, they were minimized by changing the decoupling sequence to 'bi_waltz65_256'[2].

Solid-state NMR experimental details

^{7}Li and ^{19}F NMR spectra were collected at a MAS frequency of 30 kHz, with a recycle delay of 30 s and RF field strength of 100 kHz. ^{7}Li and ^{19}F shifts were externally referenced to lithium fluoride at −1 ppm and −204 ppm, respectively.

DNP NMR experimental details

Table S1 Summary of the DNP NMR samples

Sample No.	Sample description	Sample mass (mg)	KBr (mg)	Radical solution	Radical volume (μL)	^{1}H $\epsilon_{on/off}$
1	FEC30	5.7	13.0	16 mM TEKPol in TCE/d-TCE/$CDCl_3$ (56/24/20, v/v/v)	4.0	5
2	FEC50	6.2	18.0	16 mM TEKPol in TCE/d-TCE (80/20, v/v)	4.0	16
3	$^{13}C_3$FEC100	4.0	15.0	16 mM TEKPol in TCE/d-TCE (80/20, v/v)	4.0	3
4	VC50	5.0	15.0	16 mM TEKPol in TCE/d-TCE (80/20, v/v)	4.0	13
5	LP30, 50 cycles	9.5	24.0	16 mM TEKPol in TCE	6.0	16
6	LP30, 1st cycle	5.4	14.7	16 mM TEKPol in TCE	3.5	16
7	FEC, 1st cycle	8.1	21.0	16 mM TEKPol in TCE	5.0	6
8	VC, 1st cycle	6.6	17.0	16 mM TEKPol in TCE	4.0	10

S2: Additional electrochemical data

Table S2 Summary of the electrochemical performance of SiNWs cycled in various electrolytes

Electrolytes	Capacity Retention (50^{th} discharge / 1^{st} discharge, %)	Capacity Retention (50^{th} charge / 1^{st} charge, %)	Initial Coulombic Efficiency (%)	Average Coulombic Efficiency (from 2^{nd} to 50^{th}, %)
LP30	57.95	61.45	91.73	97.8
LP30 + FEC	73.66	77.57	93.56	98.4
FEC	80.62	86.99	91.40	98.8
VC	73.45	78.89	92.48	99.1

Impedance analysis of the SEI:

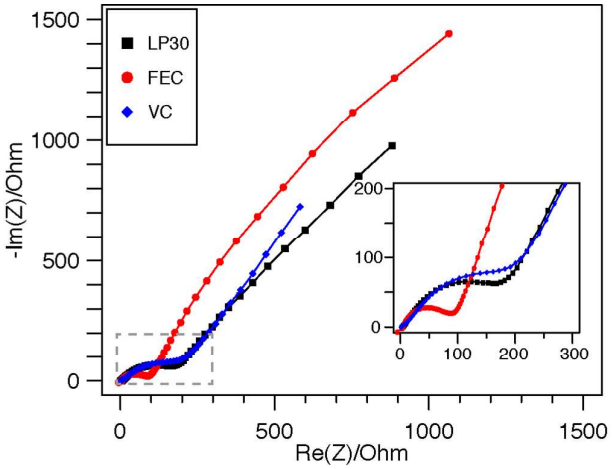

Figure S1 Electrochemical impedance spectra of SiNW half-cells after 30 cycles in LP30 standard electrolyte (black), FEC (red) and VC (blue) electrolytes in the delithiated state. The insert shows the high frequency region.

To characterize the ionic properties of the SEI formed in LP30, FEC and VC further, electrochemical impedance spectroscopy (EIS) measurements were performed on SiNWs after 30 cycles in the delithiated state. The Nyquist plots are presented in Figure S1. The depressed semicircle at high frequencies (HF) mainly reflects the charge transfer resistance (R_{ct}) of Li ions between different interphases (from the electrolyte to the SEI and from the SEI to Si), and the tail in the low frequencies region contains information about the mass transfer rate within the electrode. Note that the EIS is performed in a two-electrode system (i.e., Si vs. Li) and the interphases on the Li metal also contribute to R_{ct}.

A qualitative comparison of the size of the semicircles reveals that the FEC derived SEI has the smallest charge transfer resistance, while the VC sample even has a slightly larger R_{ct} than the LP30 sample. This agrees well with previous studies, which also showed a lower resistance for Si electrodes cycled with the addition of FEC[3,4], and an increased resistance in the presence of VC.[5] The difference of the resistance developed in the FEC and VC cells is related to the SEI thickness, the chemical structures of the SEI as well as the bonding nature between SEI and SiO_X surface. The results indicate that the FEC-derived SEI may be thinner and/or more Li^+ conductive than the SEI formed in VC and LP30 electrolytes.

Rate performance:

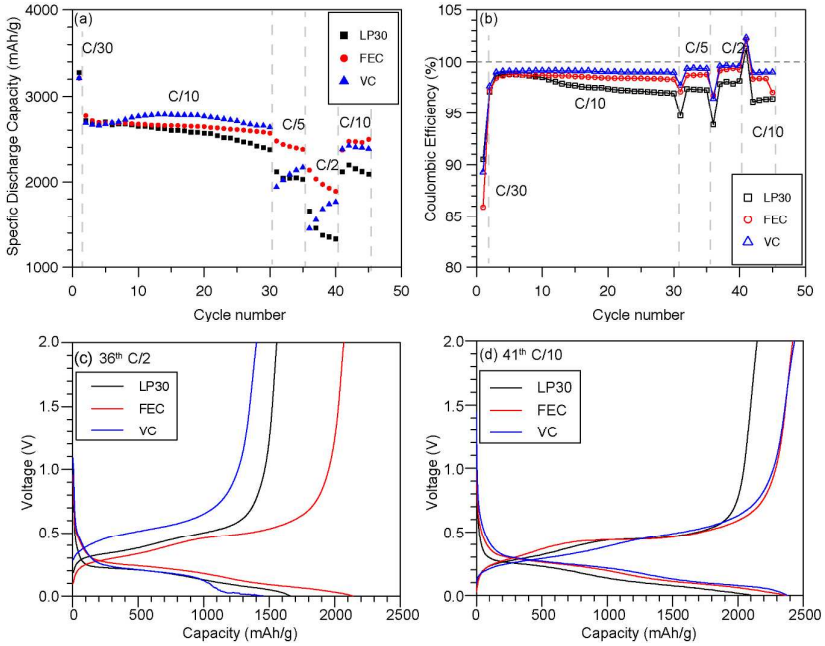

Figure S2 Rate performance of the SiNWs cycled in LP30, FEC and VC electrolyte (the 1st cycle at C/30, 2nd to 30th cycles at C/10, then cycled at C/5, C/2 and again C/10 for 5 cycles each. (a) discharge capacity and (b) Coulombic efficiency versus cycle number. Voltage curves of (c) 36th cycle at C/2, (d) 41th cycle at C/10. (1 C = 3579 mAh/g, the voltage window is 0.001 – 2 V vs. Li^+/Li)

To confirm the observations in the EIS measurements, additional rate performance tests were carried out (Figure S2). The hypothesis is that FEC samples with lower R_{ct} should have better high rate performance than LP30 and VC samples. The FEC sample indeed exhibits the highest initial capacity compared to LP30 and VC samples when they are all cycled at high rates of C/5 and C/2 (Figure S2a). However, the capacity retention trends of these samples are different. In the LP30 and FEC electrolytes, the capacity drops with each cycle, when cycling at high rates, whereas the VC sample surprisingly shows gradually increasing capacities with cycling, indicating improved Li^+ transport through the electrode structure.

To examine more closely the behavior of the VC sample at high currents, the voltage curve of the VC cell is compared to that of FEC and LP30 samples (Figure S2c and d). When cells are initially cycled at C/2 in the 36th cycle (Figure S2c), the VC sample has a larger voltage polarization than the FEC sample. During lithiation, the voltage curve of VC almost coincides with that of FEC from 2 V to 0.25 V before it quickly reaches 0.001 V at only ~1400 mAh/g. During the delithiation process, the onset for the VC sample is about 0.15 V higher than the FEC sample, and the delithiation plateau of VC is much higher than the LP30 and FEC cells. The discharge capacity of the VC sample then gradually increases when cycled at C/2 and approaching the capacity of FEC cell in the 40th cycle. The VC sample recovers its lithiation and delithiation capacities when cells are cycled at a slow rate of C/10 after high rate testing (Figure S2d), which indicates that the capacity loss is due to kinetic effects. Moreover, the VC sample consistently shows a higher Coulombic efficiency (CE) compared to LP30 and FEC samples at all current densities. The higher CE for VC electrolytes suggests that the VC-derived SEI has a better passivating ability and reduces the irreversible capacity loss during each cycle.

S3: Solution NMR data

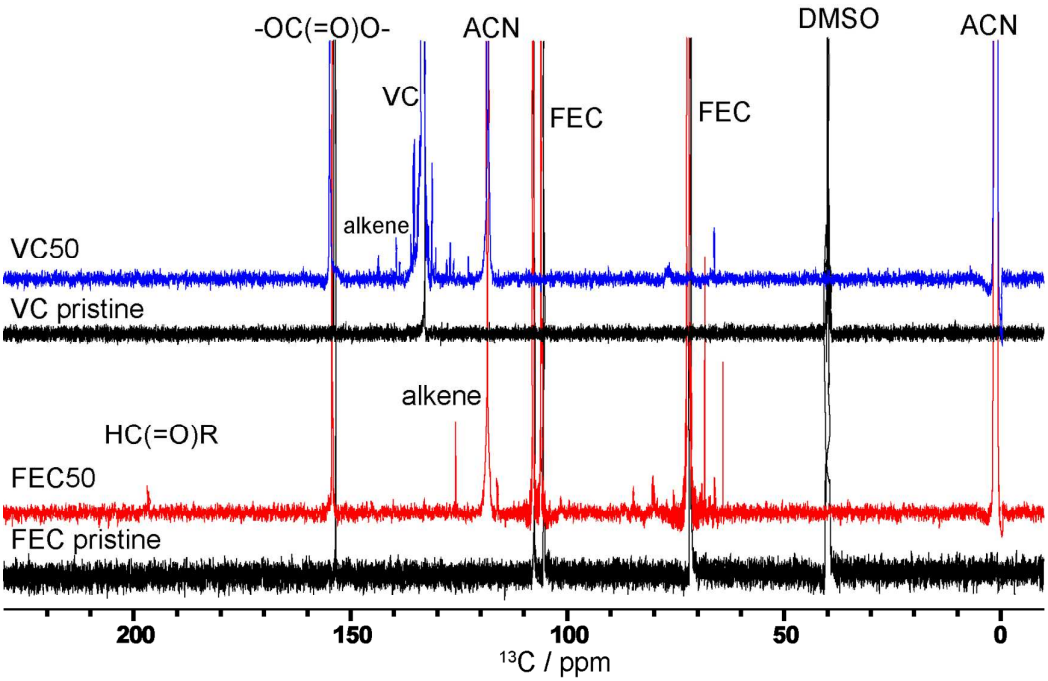

Figure S3 ^{13}C solution NMR spectra of pristine FEC, VC electrolytes and electrolytes after 50 cycles with ^{1}H decoupling.

Pristine FEC and VC electrolytes were measured in d_6-DMSO solvent, whereas the cycled FEC and VC electrolytes were measured in d_3-ACN solvent. d_3-ACN solvent was used because we observed phase separation in the cycled electrolytes and d_6-DMSO mixture.

In the cycled FEC electrolyte, new ^{13}C NMR peaks around 190 and 125 ppm appear and they are assigned to aldehyde and alkene carbon, respectively. The cycled VC electrolyte also contains additional alkene carbon species with ^{13}C shift spanning from 120-140 ppm.

S4: Additional XPS and FTIR data

XPS studies of surface species on the cycled SiNWs

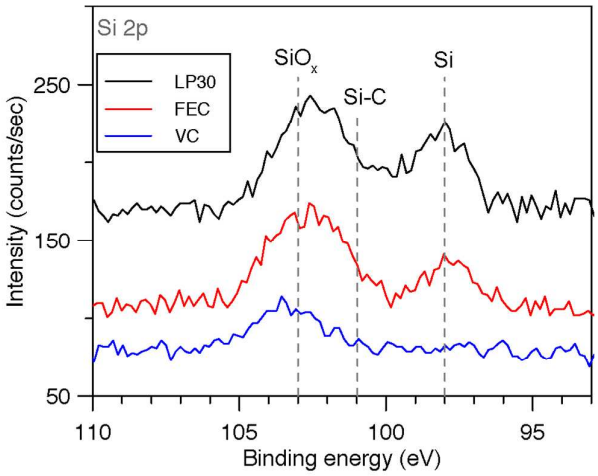

Figure S4 XPS Si 2p spectra of SiNWs cycled in different electrolyte for 30 cycles in the delithiation state.

Figure S4 shows the XPS Si 2p core peaks of SiNWs cycled in LP30, FEC and VC electrolytes after 30 cycles in their delithiated sates. All spectra contain a broad peak at ~103 eV that can be assigned to silicon oxide (SiO_x).[6] The FEC and LP30 samples both show a relatively weak peaks centered at ~98 eV that is assigned to elemental Si, whereas, no such Si peak is observed in the VC sample. All samples were measured using the same photon energy (1075 eV), and thus the Si 2p electrons for all three samples have the same inelastic mean free path (~2.5 nm). This corresponds to an information depth of ~7.5 nm (~95% of detected photoelectrons originate from within this distance of the surface) and given that the SiO_x is expected to be closer to the surface that the Si, the variations in the intensity of the elemental Si peak provide an indirect measure of the SEI thickness. The Si 2p spectra thus suggest that the VC sample has a thicker SEI than those generated from LP30 and FEC. The conclusion is consistent with McArthur et al., who used in-situ spectroscopic ellipsometry to measure the thickness of the SEI on a-Si film, and concluded that the SEI formed in electrolyte containing 2 wt% VC additive is thicker than those formed in standard electrolyte with and without 2 wt% FEC.[7] A thicker SEI will extend the Li ion diffusion pathway through the interphase before lithiation of bulk Si takes place. On the other hand, a thicker SEI potentially prevents electronic tunneling through the SEI and can better passivate the electrode. Although the thickness of SEI is an important parameter, it does not necessarily determine the electrochemistry performance. Xu et al. previously demonstrated that the desolvation process of Li ions is the rate-determining step in the lithiation of graphite instead of the diffusion rate of Li ions through the SEI.[8]

Organosilane Si-C species with a characteristic Si 2p peak at 101 eV as reported by Chan et al[9] may also be present beneath the broad peak of SiO_x in Figure S4. Fluorosilicate that has a Si 2p peak around 106 eV[10] is not clearly observable in all samples. The XPS Si 2p results are consistent with ^{29}Si NMR, showing the presence of silicate and Si-C species with little fluorosilicate on the Si surface.

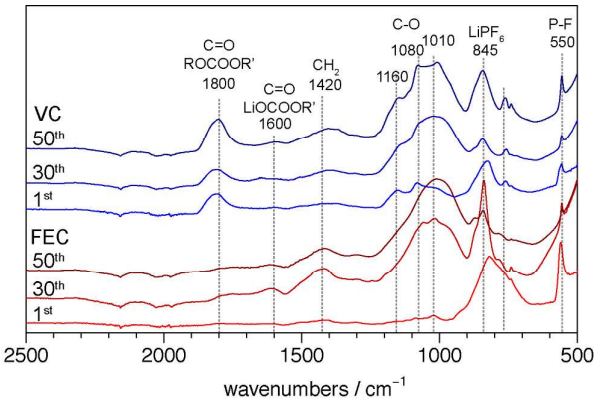

Figure S5 FTIR spectra of SiNWs cycled in 1M $LiPF_6$ in pure FEC (red) and pure VC (blue) after 1st, 30th and 50th cycles in the delithiated state without rinsing.

Figure S5 shows the FTIR spectra of the SiNWs after cycling in different electrolytes. The VC samples contain extra peaks at ~1800 cm^{-1} that can be assigned to polycarbonate groups (ROCOOR'), whereas the 1800 cm^{-1} peak is hardly observable for the all FEC samples. It is noteworthy that in Figure 2e and 2f, the carbonate species with a ^{13}C peak at 155 ppm is relatively more intense in the VC samples than the FEC samples. The presence of a polycarbonate suggests that the SEI of the VC samples contains more carbonate groups than the one formed in the FEC samples. Nie et al[11] reported similar polycarbonate groups (~1800 cm^{-1}) for Si thin film electrodes cycled in 1.2M $LiPF_6$ in pure FEC. But it was not reported whether the electrode was rinsed or not. Here the electrodes were not rinsed but dried them under dynamic vacuum overnight to remove excess solvent.

S5: inorganic SEI: ^{7}Li and ^{19}F solid state NMR

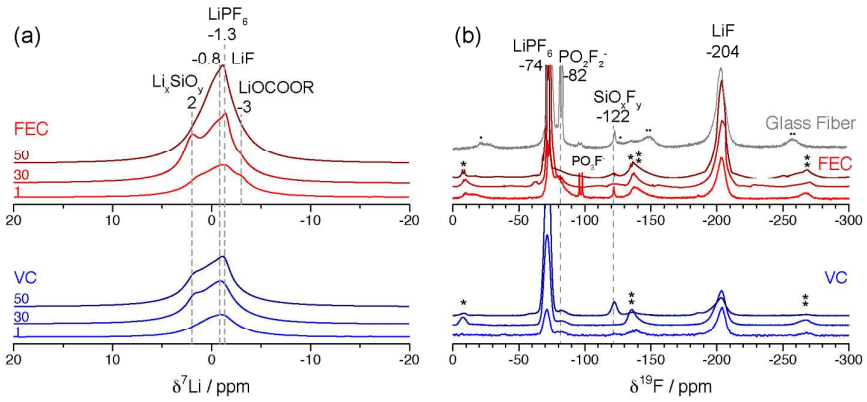

Figure S6 ^{7}Li and ^{19}F ssNMR spectra of SiNWs cycled 1M $LiPF_6$ in pure FEC or VC electrolytes after 1st, 30th and 50th cycles measured at MAS speed of 30 kHz. The grey line in (b) is ^{19}F NMR spectra of glass fiber separator after 50 cycles in FEC electrolytes measured at MAS of 25 kHz. Spinning sideband are marked with asterisks and dots.

In the ^{19}F NMR spectra of FEC sample after 1st cycle, the −97 ppm (doublet, J=1063 Hz) is assigned to POF_3^-, which forms due to the hydrolysis of PF_6^-.[12]

S6: Additional ^{13}C DNP MAS NMR data

Figure S7 shows the ^{1}H-^{13}C CP NMR of the SiNW cycled in non-enriched pure FEC electrolyte after 30 cycles. The red spectrum is measured by conventional ssNMR at room temperature and it contains three major features: an intense carbon peak at 69 ppm, which is assigned to ethylene oxide carbons, a pronounced aliphatic carbon signals between 30-40 ppm, and a small peak at around 100 ppm that can be assigned to a cross-linking carbon. To improve the signal to noise ratio, we measured the same sample using DNP NMR at 100 K. The inset in Figure S7shows that there is an extra peak at 127 ppm in this sample, which can be assigned to an alkene carbon. However, we note that these sp^2 hybridized carbons are present in extremely low concentrations compared to the other ethylene oxide and aliphatic carbons. Figure S8 shows the ^{1}H-^{13}C HETCOR of the same sample and Table S3 summarizes all the signals found in the HETCOR spectrum.

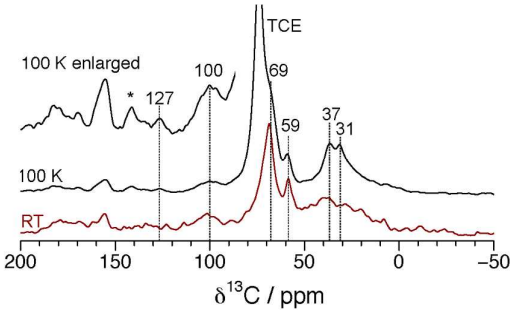

Figure S7 ^{1}H-^{13}C CP NMR spectra of SiNW cycled in 1 M $LiPF_6$ in FEC for 30 cycles. The red spectrum was measured with conventional ssNMR at room temperature at 500 MHz, the black spectrum was measured with DNP NMR at 100 K. The inset (top, left) shows the enlarged, 100 K DNP NMR spectrum that reveals an extra peak at 127 ppm. Spinning sidebands are marked with an asterisk.

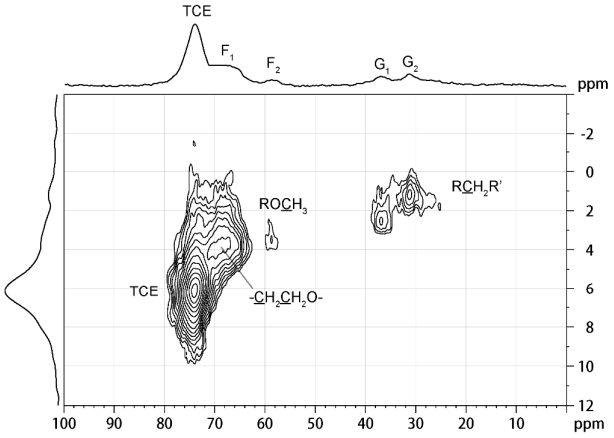

Figure S8 ^{1}H-^{13}C DNP HETCOR of SiNWs cycled in 1M $LiPF_6$ in FEC for 30 cycles. Contact time of 200 µs is used.

Table S3 Summary of HETCOR peaks in Figure S8

Label	^{13}C /ppm	^{1}H/ppm	Possible assignment
TCE	74	6.1	TCE
F1	70	4.1	-CH_2***CH***$_2$O-
F2	59	3.5	RO***CH***$_3$
G1	37	2.3	R***CH***R_2'
G2	31	1.3	R***CH***$_2$R'

Table S4 Summary of the peaks in ^{13}C-^{13}C correlation spectrum (Post-C7)

Molecular Fragments	SQ Shift /ppm	SQ Shift /ppm	DQ Shift / ppm	Sum /ppm
A_1-A_2	35.2	31.3	64.9	66.5
B_2-A_4	75.3	35.5	106.4	110.8
B_2'-B_3	75.6	69.9	142.1	145.5
B_1-A_3	76.3	17	91.6	93.3
C_1-A_5	97.8	33.8	130.7	131.6
C_2-B_4	101.8	71.9	172.2	173.7

S7: Additional ^{29}Si DNP MAS NMR data

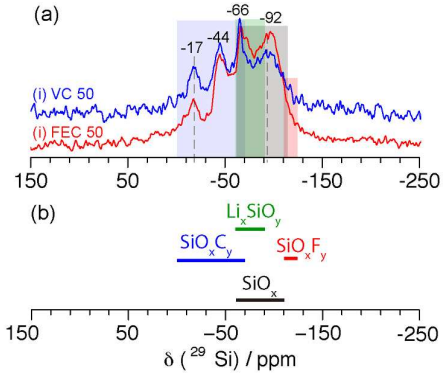

Figure S9 ^{1}H-^{29}Si CP DNP NMR spectra of SiNW cycled in VC, FEC after 50 cycles (a), (b) chemical shift ranges of organosilicate[13], silicate, lithium silicate and fluorosilicate[14].

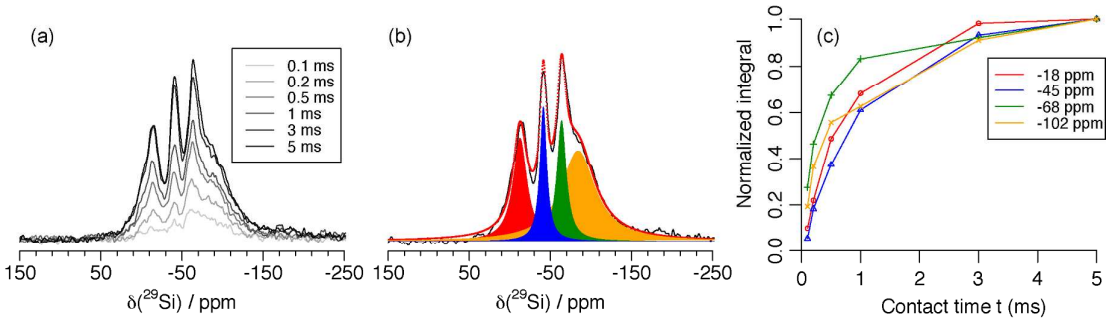

Figure S10 ^{1}H-^{29}Si CP DNP NMR spectra of SiNWs cycled LP30 for 50 cycles with various contact times (a), the deconvoluted spectrum (b), the build-up curve of each deconvoluted peak (c).

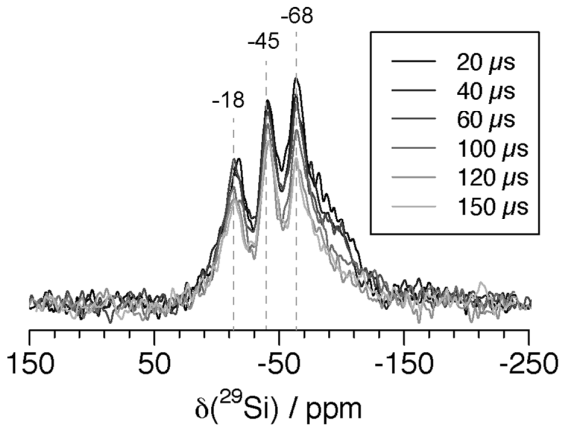

Figure S11 Spectra of ^{1}H-^{29}Si dephasing experiments of SiNWs cycled with LP30 for 50 cycles, spinning at 12.5 kHz.

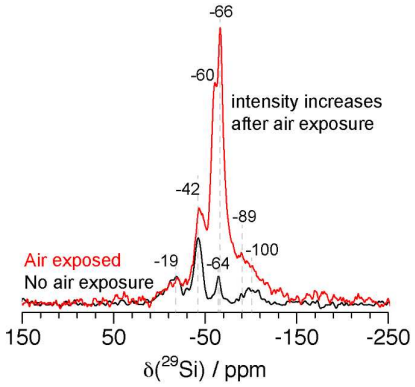

Figure S12 ^{1}H-^{29}Si CP DNP NMR spectra of SiNWs cycled in FEC for 100 cycles before air exposure (black) and after air exposure (red).

S8: Additional cycling data

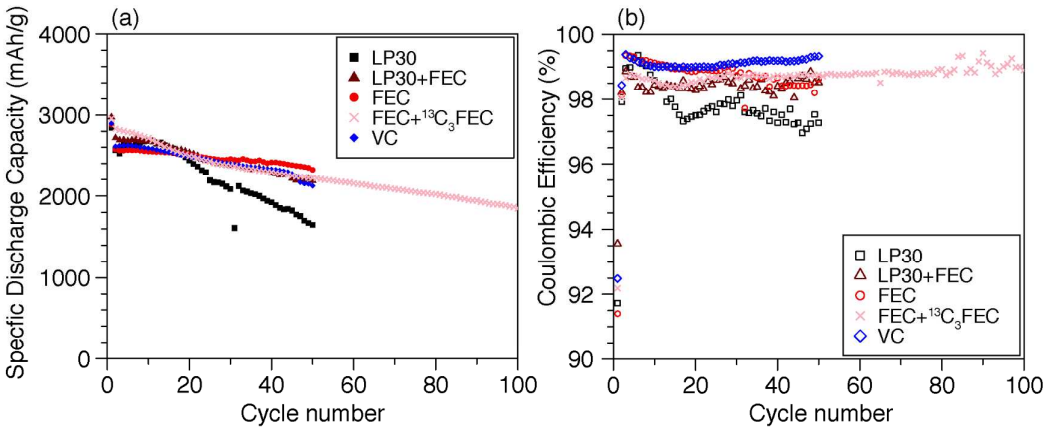

Figure S13 Electrochemical performances for SiNWs cycled in FEC+$^{13}C_3$ FEC and the results from representative SiNWs cycled using the electrolyte formulations listed in Table 1. (a) Specific lithiation capacity and (b) Coulombic efficiency versus cycle number.

The initial CE of the $^{13}C_3$ FEC sample is 92.2 %, which is slightly higher than the CE of the sample prepared with the non-enriched FEC sample (91.4 %) presented here, but this difference is within the error associated with variations in the SiNWs electrodes (see below), which are synthesized individually by CVD methods. Due to the small amount of $^{13}C_3$ FEC available, the water content in this electrolyte was not directly determined. But on the basis of the similar electrochemical results, the $^{13}C_3$ FEC sample has a similar water content as the FEC sample obtained from Sigma.

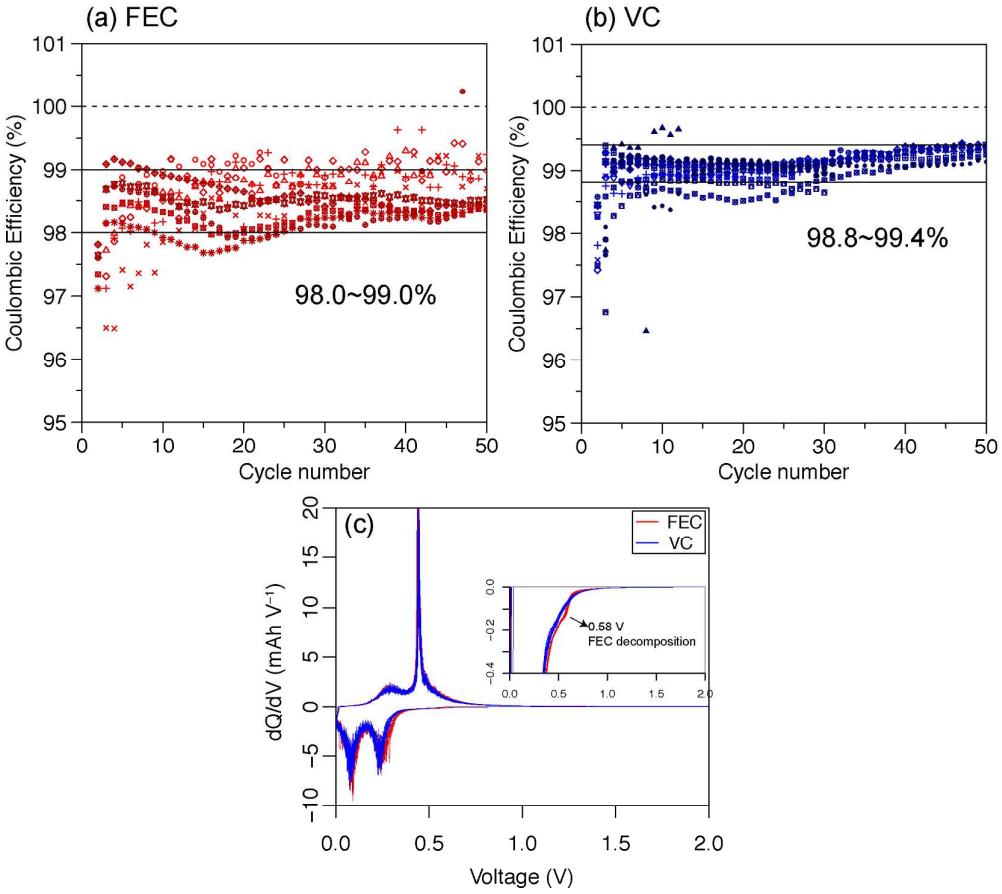

Figure S14 (a-b) The Coulombic efficiencies of multiple SiNWs cells cycled in1M $LiPF_6$ in pure FEC and VC electrolytes. (c) dQ/dV from 30^{th} to 50^{th} cycles of cells cycled in FEC and VC electrolytes (FEC in red, VC in blue).

Experiments were performed to assess the effect of variations between SiNW electrodes on the electrochemistry, since the SiNWs were synthesized individually by CVD methods in different batches. Coulombic efficiencies (CE) of multiple cells used in this study are shown in Figure S14 a and b. SiNWs cells cycled in FEC have CEs in the range of 98.0 - 99.0%, whereas, cells cycled in VC electrolyte show a higher CEs (98.8% - 99.4%). While variations are observed, the VC samples systematically show higher CEs.

Figure S14c compares the dQ/dV plot of cells cycled in FEC and VC electrolytes. An extra peak at 0.58 V is clearly observed in the FEC sample, indicating FEC is continuously being decomposed as no lithiation of Si occurs in this voltage. The result is consistent with the lower CEs observed in the FEC samples compared to the VC samples, suggesting that VC forms a more stable SEI than FEC.

S9: DFT calculation results

Computational details

Density Functional Theory (DFT) calculations were run on a set of molecules that correspond to some of the proposed polymer building blocks of the SEI system. To explore the effect of alkane chain length on the chemical shift, the carbon chains were extended systematically, from R=Me to R=Pr (in essence Et and Pr for the inner linear part). Another set of molecules was also created with a cyclic carbonate functional group. Both of these structures can be seen in Figure S15, where the main carbon of interest has been made explicit in red.

In each case, the calculations were performed using Orca 4.0.1.2[15]. The PBE0 functional[16] with the def2-TZVP[17] basis set was used for the geometry optimization of the molecules. NMR calculations were performed with the same functional and the pcSseg-2[18] basis set. The TightSCF option was also used. The same procedure was used for the calculation of the reference, tetramethylsilane (TMS).

Figure S15. The branched (left) and cyclic systems (right) used for DFT/NMR calculations. The acetal carbon of interest is emphasized in the structures.

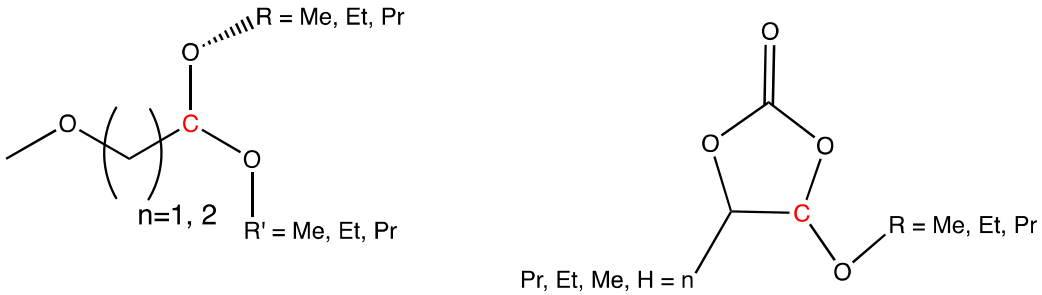

The resulting chemical shifts are given in Table S5 and S6. The acetal carbons of the cyclic molecules have ^{13}C shifts ranging from 104.8 to 114.0 ppm (Table S5). The addition of an alkyl group to the cyclic structure shifts the ^{13}C acetal peak considerably by ~5 ppm (e.g. from 106.0 ppm to 111.2 ppm).

The branched systems span a shift range between 107.6 to 113.4 ppm. Comparing the ethyl and propyl cores (n=1 and 2 in Table S6) there is a small, yet clear, trend of a smaller ^{13}C shift for structure containing propyl cores. Changing the R, R' groups does not result in a clear trend here.

These results are in line with the experimental values that are assigned in the paper: acetal carbon in the cyclic structure has higher ^{13}C shift than acetal carbons in the branched structure).

Table S5: The calculated ^{13}C chemical shifts of the cyclic acetal carbons of Figure S14 (where n and R are defined). In each case, TMS is used as a reference.

n	R	Δ [ppm]	n	R	Δ [ppm]	n	R	Δ [ppm]	n	R	Δ [ppm]
H	Me	106.0	Me	Me	111.2	Et	Me	111.0	Pr	Me	111.1
H	Et	104.8	Me	Et	110.0	Et	Et	109.8	Pr	Et	113.1
H	Pr	105.1	Me	Pr	110.4	Et	Pr	110.3	Pr	Pr	114.0

Table S6: The calculated ^{13}C chemical shifts of the branched acetal carbons of **Figure S15** (where n, R and R' are defined). In each case TMS is used a reference.

n	R	R'	Δ [ppm]	n	R	R'	Δ [ppm]
1	Me	Me	109.9	2	Me	Me	109.0
1	Me	Et	108.8	2	Me	Et	107.6
1	Me	Pr	109.8	2	Me	Pr	108.4
1	Et	Me	110.3	2	Et	Me	109.4
1	Et	Et	109.0	2	Et	Et	108.2
1	Et	Pr	108.7	2	Et	Pr	107.9
1	Pr	Me	110.0	2	Pr	Me	109.4
1	Pr	Et	109.1	2	Pr	Et	108.1
1	Pr	Pr	113.4	2	Pr	Pr	107.8

Reference:

(1) Piotto, M.; Bourdonneau, M.; Elbayed, K.; Wieruszeski, J.-M.; Lippens, G. *Magn. Reson. Chem.* **2006**, *44*, 943–947.
(2) Zhou, Z.; Kümmerle, R.; Qiu, X.; Redwine, D.; Cong, R.; Taha, A.; Baugh, D.; Winniford, B. *J. Magn. Reson.* **2007**, *187*, 225–233.
(3) Etacheri, V.; Haik, O.; Goffer, Y.; Roberts, G. a.; Stefan, I. C.; Fasching, R.; Aurbach, D. *Langmuir* **2012**, *28*, 965–976.
(4) Schroder, K.; Alvarado, J.; Yersak, T. a.; Li, J.; Dudney, N.; Webb, L. J.; Meng, Y. S.; Stevenson, K. J. *Chem. Mater.* **2015**, *27*, 5531–5542.
(5) Hu, Y. S.; Demir-Cakan, R.; Titirici, M. M.; Müller, J. O.; Schlögl, R.; Antonietti, M.; Maier, J. *Angew. Chemie - Int. Ed.* **2008**, *47*, 1645–1649.
(6) Nakai, H.; Kubota, T.; Kita, A.; Kawashima, A. *J. Electrochem. Soc.* **2011**, *158*, 798–801.
(7) McArthur, M. A.; Trussler, S.; Dahn, J. R. *J. Electrochem. Soc.* **2012**, *159*, A198–A207.
(8) Xu, K.; Cresce, A. Von; Lee, U. *Langmuir* **2010**, *26*, 11538–11543.
(9) Chan, C. K.; Ruffo, R.; Hong, S. S.; Cui, Y. *J. Power Sources* **2009**, *189*, 1132–1140.
(10) Philippe, B.; Dedryvèire, R.; Gorgoi, M.; Rensmo, H.; Gonbeau, D.; Edström, K. *J. Am. Chem. Soc.* **2013**, *135*, 9829–9842.
(11) Nie, M.; Abraham, D. P.; Chen, Y.; Bose, A.; Lucht, B. L. *J. Phys. Chem. C* **2013**, *117*, 13403–13412.
(12) Wilken, S.; Treskow, M.; Scheers, J.; Johansson, P.; Jacobsson, P. *RSC Adv.* **2013**, *3*, 16359.
(13) Widgeon, S. J.; Sen, S.; Mera, G.; Ionescu, E.; Riedel, R.; Navrotsky, A. *Chem. Mater.* **2010**, *22*, 6221–6228.
(14) Hoffner, F. M.; Delmotte, L.; Kessler, H. *Zeolites* **1993**, *13*, 60–63.
(15) Neese, F. *Wiley Interdiscip. Rev. Comput. Mol. Sci.* **2018**, *8*, 4–9.
(16) Perdew, J. P.; Ernzerhof, M.; Burke, K. *J. Chem. Phys.* **1996**, *105*, 9982–9985.
(17) Weigend, F.; Ahlrichs, R. *Phys. Chem. Chem. Phys.* **2005**, *7*, 3297.
(18) Jensen, F. *J. Chem. Theory Comput.* **2015**, *11*, 132–138.